Relaxor Ferroelectrics: Back to the Single-Soft-Mode Picture

B. Hehlen,[1,*] M. Al-Sabbagh,[1] A. Al-Zein,[2] and J. Hlinka[3,†]
[1]Laboratoire Charles Coulomb (L2C) UMR CNRS 2251, University of Montpellier, 34095 Montpellier, France
[2]European Synchrotron Radiation Facility, BP 220, F-38043 Grenoble Cedex, France,
and Physics Department, Faculty of Science, Beirut Arab University (BAU), Beirut, Lebanon
[3]Institute of Physics, The Czech Academy of Sciences, Na Slovance 2, 18221 Praha 8, Czech Republic
(Received 30 May 2016; published 7 October 2016)

The fluctuations of electric polarization in a disordered ferroelectric substance, relaxor crystal $PbMg_{1/3}Nb_{2/3}O_3$ (PMN), were studied using a nonlinear inelastic light-scattering technique, hyper-Raman scattering, within a 5–100 cm^{-1} spectral interval and in a broad temperature range from 20 to 900 K. The split ferroelectric mode reveals a local anisotropy of up to about 400 K. Spectral anomalies observed at higher temperatures are explained as due to avoided crossing of the single primary polar soft mode with a temperature-independent, nonpolar spectral feature near 45 cm^{-1}, known from Raman scattering. The temperature changes of the vibrational modes involved in the measured fluctuation spectra of PMN were captured in a simple model that accounts for the temperature dependence of the dielectric permittivity as well. The observed slowing down of the relaxational dynamics directly correlates with the huge increase of the dielectric permittivity.

DOI: 10.1103/PhysRevLett.117.155501

A large variety of ferroelectric relaxors originate from the generic perovskite structure ABO_3 in which the single B-type ion is replaced by a mixture of B' and B'' cations [1]. These complex perovskite crystals exhibit broad and frequency-dependent peaks in their dielectric response, associated with a huge value of the static dielectric constant without any long-range polar ordering [2–6]. The origin of these behaviors is debated [3,7–12]. One popular scenario is the formation of randomly oriented polar nanoregions (PNRs) at high temperature [3,13–15]. Owing to the $\{B'B''\}$ chemical disorder, these nanoregions do not grow into macroscopic domains below the Curie-Weiss temperature T_0, as in the usual ferroelectric substances [16]. Such a kind of disorder at nanoscale places relaxors at a very interesting frontier position between crystals and disordered systems. Indeed, although perfectly crystalline macroscopically, they exhibit most of the universal properties of glasses, motivating many theoretical [17–22] and experimental investigations [7,23–26].

Within that family, lead magnesium niobate, $PbMg_{1/3}Nb_{2/3}O_3$ (PMN), is a textbook example. Its structure remains cubic in average down to the lowest temperatures [14]. It has been proposed that the formation of dynamical PNRs occurs around the Burns temperature $T_d \simeq 620$ K [27,28], that they start to become static around $T^* \simeq 400$–500 K [29–33], and that their dynamics slows down until $T_f \sim 220$ K [7,34] (see Fig. 1). Many spectroscopic experiments have been performed in an attempt to relate these assumptions to the dynamical phenomena. These investigations include neutron scattering [35–39], Raman scattering [40], and infrared absorption [41] experiments. Another technique, hyper-Raman scattering (HRS) [42], is particularly suitable for probing the low-frequency polar modes in nonpolar crystal phases [43,44]. The most important outcome of HRS studies of relaxors [45–47] was a neat observation of the two low-frequency anharmonic modes [45] in the vicinity of T_d. These two modes were associated with the two components of the soft mode, split by the local polar anisotropy [48].

However, these findings raised new questions, such as the following: Are there one or two soft modes well above T_d, when the material is in its paraelectric state [35,39]? How do these excitations relate to the vibrations observed below T_f [40,41,49]? What is the nature of the quasielastic

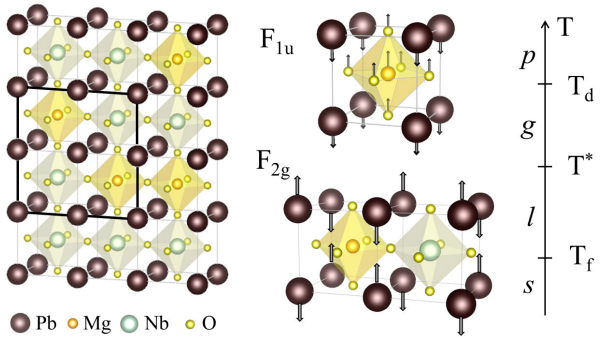

FIG. 1. Structure of complex perovskites. Left: B' and B'' atoms are distributed randomly so that on average, the crystal has a cubic $Pm\bar{3}m$ structure. Some experiments indicate the presence of $Fm\bar{3}m$ (checkerboard-ordered) clusters (bold square). Middle: Eigenvectors of the low-frequency vibrations emphasizing the in-phase motion (F_{1u} mode) and the out-of-phase (F_{2g} mode in the $Fm\bar{3}m$-symmetry cluster) motion of the lead atoms. Right: Characteristic temperatures delimiting regions of normal paraelectric (p), dipole gas (g), dipole liquid (l), and dipole ice (s) relaxor states, respectively.

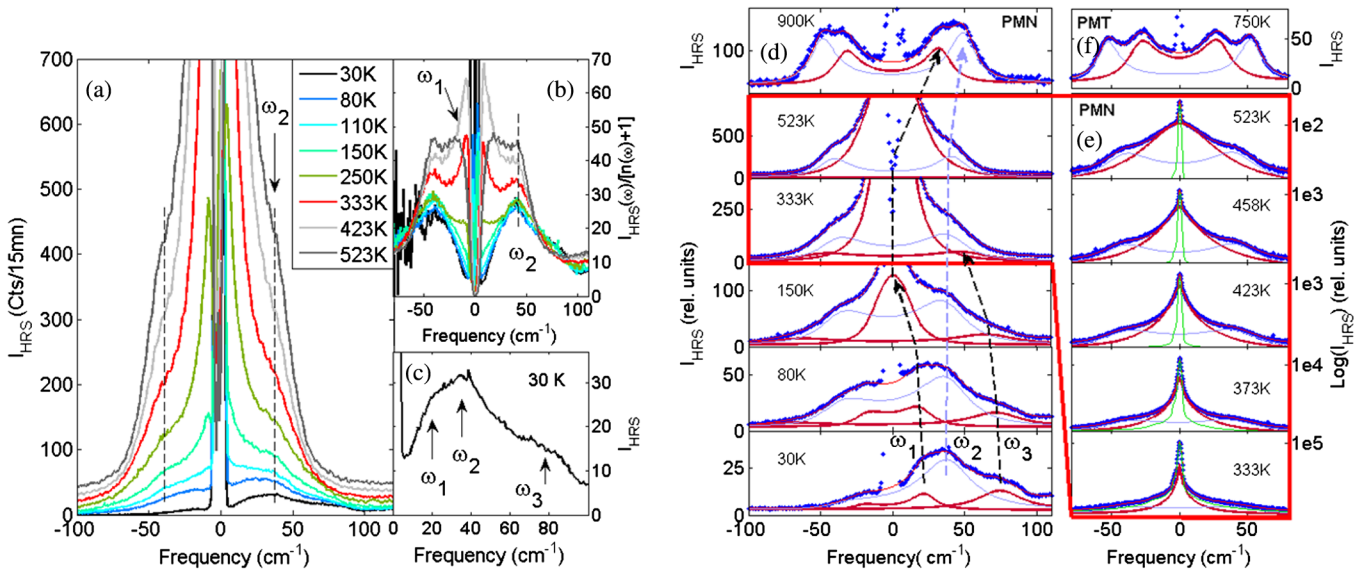

FIG. 2. Hyper-Raman spectra and their fit: (a) Temperature dependence of the HRS intensity, I_{HRS}. (b) Same spectra normalized by the Bose factor emphasizing an almost T-independent behavior of ω_2. (c) Zoom of the spectra at 30 K showing *three* modes at low temperature. (d) Fit of the HRS spectra of PMN from 30 K to 900 K. (e) High resolution spectra (in log scale) in the temperature domain where the soft mode (ω_1) is overdamped. (f) Spectrum of PMT at 750 K.

peak observed in between T_f and T^* [30,50], where the dielectric response exhibits its maxima [41]? Such questions could not be answered by HRS experiments at that time because the basic experimental setup as described in Refs. [46,47] allowed us to probe the soft mode spectra of PMN only in a limited range of temperatures around T_d. To resolve these issues, previous measurements are completed here with three additional HRS experiments, each designed to deal with a particular experimental difficulty, associated with (i) the presence of strong elastic scattering below T_f, (ii) the strong blackbody radiation background at temperatures well above T_d, and (iii) the extreme spectral resolution requirements in the intermediate temperature range around T^*.

First, the low-temperature spectra had to be recorded using an ultranarrow notch filter to reduce the strong elastic (hyper-Rayleigh) line, and a filter positioned at the exit of the laser to remove the residual background on the tail of the laser spectral line. The combination of both allowed us to measure inelastic responses as weak as 1 count/mn at peak maxima down to ± 8 cm^{-1}. This gave us a new possibility, to inspect the low-temperature HRS spectra of PMN (Fig. 2). One observes three modes at 30 K, labeled ω_i, $i = 1, \ldots, 3$ by increasing frequencies. Modes ω_1 and ω_2 are very close to each other but they could be distinguished by their different polarized HRS efficiencies. Figure 2(b) shows the HRS spectra normalized by the Bose-Einstein population factor. This representation reveals that the ω_2 mode has practically the same frequency and spectral shape at any temperature there, while the ω_1 mode is strongly *temperature dependent* and it gradually collapses into the elastic (hyper-Rayleigh) line upon heating. An additional mode with frequency ω_3 [see Fig. 2(c)] can be followed roughly to room temperature [see Fig. 2(d)]. The spectra have been fitted assuming damped harmonic oscillators (DHOs) for the three vibrations. The results are shown in Figs. 2(d) and Fig. 3.

Second, raw HRS spectra of PMN taken at temperatures above ~750 K suffer from a sizable background signal arising from the blackbody radiation. However, it turned out that this background can be measured independently at each temperature and removed from the spectra. In this way, we could study the two earlier reported paraelectric soft modes [45] up to 900 K [see the top of Fig. 2(d)]. Their frequencies, obtained from the fits with DHO formulas, disclosed an unexpected change in the temperature trend (ω_1 and ω_2 in Fig. 3), typical for the avoided crossing phenomenon. Moreover, two underdamped paraelectric soft modes with similar temperature dependence were also found in $PbMg_{2/3}Ta_{1/3}O_3$ (PMT), [Figs. 2(f) and 3], indicating that this avoided crossing is a common feature of cubic relaxors.

Third, we have pushed the limits of the HRS technique to access the spectral response of the lowest frequency ω_1 mode between T_f and T^*, where it transforms into an overdamped excitation and where it manifests as a quasielastic scattering. Since the truly elastic scattering intensity (hyper-Rayleigh) increases there as well, the experimental setup was modified in order to allow signal detection with a very high dynamical range and also a high spectral resolution, at the expense of the overall intensity reduction. A logarithm plot of such HRS spectra is presented in Fig. 2(e). The profile of the elastic component, which defines the apparatus resolution function, has been measured independently at 20 K, a temperature at which the inelastic signal is negligible. The fits include two DHOs (ω_1 and ω_2, respectively) and a delta function at zero

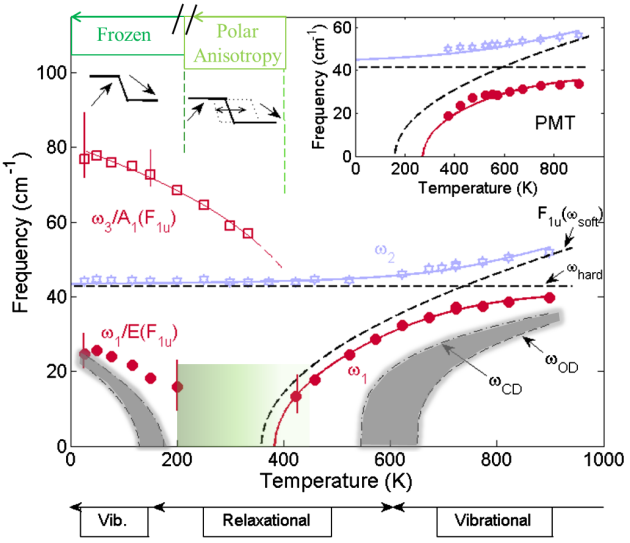

FIG. 3. Mode splittings and mode couplings: Temperature dependence of the modes ω_1, ω_2, and ω_3, observed by HRS. The limit at $\omega = 0$ of the two gray regions defines the crossovers from the vibrational to the relaxational regime of the polar ω_1 vibration. The splitting of the latter into A_1 and E vibrations is the likely signature of the growth of a polar anisotropy on cooling below ~400 K. The full and dashed lines associated with $\{\omega_1, \omega_2\}$ and $\{\omega_{soft}, \omega_{hard}\}$, respectively, result from a mode-coupling model (see text). The same model successfully applies to PMT (inset).

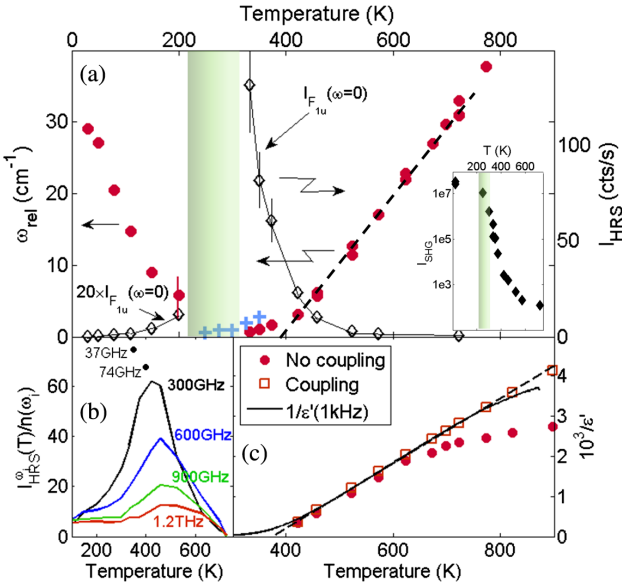

FIG. 4. Soft polar dynamics and dielectric response. (a) The slowing down of the polarization dynamics in PMN is highlighted by (i) the lowering of the soft mode relaxational frequency (circles, ω_{rel}) down to ~0.7 cm^{-1}, (ii) the divergence of its response at $\omega = 0$ [diamonds, $I_{F_{1u}}(\omega = 0)$], and (iii) the rise of the total intensity at $\omega = 0$ (I_{SHG} in the inset). For comparison, the cross symbols (+) in and near the shaded region stand for the neutron spin-echo data [25]. (b) Temperature dependence of the dielectric response at THz frequencies as extracted directly from the HRS data (arbitrary units). The maxima of $\epsilon(T)$ at 34 GHz and 74 GHz (circle) are reproduced from dielectric measurements of Ref. [41]. (c) Inverse permittivity of PMN at 1 kHz, obtained from dielectric measurement (line) and recalculated from the HRS data with (squares) and without (circles) mode coupling. Dashed lines in panels (a) and (c) are guides to the eyes emphasizing a linear behavior.

frequency, all convoluted with the apparatus function. The frequency ω_1 has been extracted down to ~420 K. For temperatures below, the soft mode damping Γ_1 becomes so large that the spectral line shape does not allow estimation of ω_1^2 and Γ_1 independently. Therefore, only their ratio $\omega_{rel} = \omega_1^2/\Gamma_1$, corresponding to half width of the ω_1 mode spectral response, was considered as the remaining reliable parameter (for further clarification and comparison, see, e.g., Refs. [44,45,51]). This soft mode relaxational frequency ω_{rel} could be reliably estimated down to about 330 K (see Fig. 4).

The temperature dependence of the frequencies of the three modes is compiled in Fig. 3. The above mentioned idea of the avoided crossing differs from the previous scenarios (Refs. [38,39,48]) and implies that the temperature dependence of ω_1 and ω_3 may originate from a single soft mode and a single hard mode. Indeed, the measured temperature course of ω_1 and ω_2 can be nicely adjusted to the square roots of the eigenvalues of a 2×2 dynamical matrix, describing a single bare soft mode, with the Cochran-law temperature dependence ($\omega_{soft} = A\sqrt{T - T_0}$), coupled to a mode with T-independent frequency ω_{hard}, through a T-independent coupling Δ. The temperature course of the bare and dressed frequencies is plotted in Fig. 3 with dashed and full lines, respectively; calculations correspond to $\omega_{hard} = 42.7$ cm^{-1}, $T_0 = 358$ K, $\Delta = 944$ cm^{-1}.

The ω_{hard} mode appears to be intrinsically a nonpolar mode, because it is not influenced by the temperature crossovers between subsequent relaxor states. Therefore, it can be assumed that the dielectric strength is attached only to the ω_{soft} mode. Within such coupling model, the overall low-frequency dielectric permittivity ϵ_0 can be then expressed as [52]

$$\epsilon_0 = \epsilon_\infty + \frac{\Omega_{soft}^2}{\omega_{soft}^2 - \left(\frac{\Delta}{\omega_{hard}}\right)^2}, \quad (1)$$

where Ω_{soft} is the plasma frequency of the bare soft mode. With reasonable values for the high frequency dielectric constant, $\epsilon_\infty = 25$, and for the plasma frequency $\Omega_{soft} = 735$ cm^{-1} [4], the above formula reproduces very well the experimental data for the static permittivity [Fig. 4(b)]. Note that if instead the same dynamical dipole moment (the plasma frequency Ω_{soft}) would be assigned directly to the ω_1 mode, the derived inverse permittivity [inverse of $\epsilon_\infty + (\Omega_{soft}/\omega_1)^2$ shown by full circles in Fig. 4(c)] would be a clearly concave function of temperature even in the temperature region where the direct dielectric measurements show an essentially Curie-Weiss (linear) behavior [full line in Fig. 4(c)]. This comparison gives additional support to the present coupled-mode model, where the ferroelectric F_{1u} Last-type [4] (Fig. 1) soft mode is identified with the *bare* ω_{soft} mode.

The magnitude of ω_{hard} and its almost constant temperature behavior over the whole investigated temperature range suggests its close correspondence with the strongest low-frequency band in Raman spectra [31,40,53–55]. This Raman band is often assigned to the F_{2g} optic mode of the idealized $Fm\bar{3}m$ ($Z = 2$) structure with a rocksalt B-site ordering. This F_{2g} mode is actually an acousticlike mode folded from the Brillouin zone corner of the parent $Pm\bar{3}m$ ($Z = 1$) structure, what explains its temperature stability and rather low frequency. However, in the presence of considerable B-site occupational fluctuations [56], it is reasonable to assume that the $Fm\bar{3}m$ ($Z = 2$) symmetry is strongly perturbed and many other modes from the flat part of the acoustic phonon branches near the Brillouin zone boundary are contributing to this Raman band. This disorder also allows for the bilinear coupling between the two bare modes of intrinsically different symmetry.

The upper and lower limits of the gray regions in Fig. 3 stand for the maximum of the DHO spectral response (ω_{OD}), and for the undamped frequency (ω_{CD}), respectively [45]. In the temperature interval where these quantities are vanishing, the polar soft mode exhibits a relaxational behavior and the most relevant frequency scale is its relaxation frequency ω_{rel}. Here it is realized roughly between T_f and T_{d}. The narrowing of the soft mode line shape, decreasing ω_{rel}, and the concomitant divergence of the soft mode scattering intensity $I_{F_{1u}}$ at $\omega = 0$ when approaching T_f are the signatures of the slowing down of the polarization dynamics [Fig. 4(a)]. The relaxations measured by neutron spin echo in the overdamped regime [25] are also compared to our data in Fig. 4(a). The values of the inverse relaxation time match rather well with ω_{rel} implying that both techniques are probing the same overdamped soft mode rather than two distinct dynamical components (as seen, e.g., near the ferroelectric phase transition of $BaTiO_3$ [52,57]). Note that qualitatively, the two temperature crossovers between the vibrational and overdamped dynamics reported here are compatible with the previous observations in optical and neutron scattering experiments. Most likely, the HRS technique reveals the relevant spectral details more neatly because it happened to simultaneously yield a better spectral resolution and dynamical range of detectable scattering intensity.

In the spirit of the new model, the overdamped soft mode observed in our experiments should determine the dielectric properties of PMN in a broad temperature range. It is well known that the fixed-frequency dielectric permittivity of PMN peaks at a temperature T_{max}, that increases with the measuring frequency: it is close to T_f when in ultraslow measurements in mHz frequency range and it approaches about 400 K for the dielectric response detected at a few hundreds of GHz [41]. Such an extremely broad frequency range is not accessible by the HRS technique. Nevertheless, for frequencies in the THz range, we could directly extract from our spectra the temperature dependence of the HRS soft mode response intensity, corrected for the Bose-Einstein factor [see Fig. 4(b), the contribution of the ω_2 mode was removed]. The intensity maxima T_{max} of such reduced HRS intensity plots clearly merge well with the T_{max} values of the previous GHz-range dielectric measurements, as expected.

The polar nature of the modes observed in the HRS experiment is also corroborated by a reasonable correspondence of the ω_1 and ω_3 frequencies with their counterparts detected directly by IR spectroscopy below T_f [41]. These two modes have an opposite trend than that of the high-temperature soft mode, and they have been therefore assigned to the A_1 and E components of the ferroelectric soft mode, renormalized and split by the presence of the static polarization. Present experiments give clear evidence of the A_1-E splitting up to about 400 K, suggesting the polar anisotropy persists well above the freezing temperature T_f. However, our data do not support the continuity between ω_2 and ω_3 branches, conjectured in previous works [35,45].

In addition, the steepest temperature dependence of the second harmonic signal I_{SHG} (total intensity scattered at $\omega = 0$), presumably related to the overall polarization of the lattice, is observed well above the T_f temperature [see the inset of Fig. 4(a)]. These findings thus indicate that T_f is much more likely related to the freezing of the dynamics of the nanodomain polar boundaries rather than with the volume freezing of the polarization itself, because the latter appears to be already frozen near T^*.

In summary, the state-of-the-art HRS experiments accomplished here yielded a comprehensive picture of THz-range polarization dynamics in a PMN perovskite relaxor. The dynamical signature changes with temperature [9,58]. (i) At temperatures above T_d, we have identified a single intrinsic soft mode, as expected for a normal paraelectric phase. The mode is underdamped and the only anomaly is the clear signature of mixing with a nonpolar, disorder-induced hard mode. (ii) Between T_d and T^*, the dressed soft mode clearly continues to soften ($d\omega_1/dT > 0$) and it largely accounts for the low-frequency dielectric properties. Its dynamics acquires a relaxational character, but there is no evidence for dipole condensation yet. The effects ascribed usually to the so-called dynamic polar nanoregions or lead off-centering are probably just due to the fluctuations of this soft mode. This stage could be considered as a dipole gas state (g in Fig. 1). (iii) HRS spectra taken in the dipole liquid stage between T^* and T_f (l in Fig. 1) are consistent with the picture of the soft mode split in two components, both having the reversed temperature dependence ($d\omega/dT < 0$). Such a temperature trend and the polar anisotropy suggests that the bulk polarization is largely condensed. It also suggests that the observed high dielectric response with a broad spectrum of relaxation times can be understood as due to mobile interfaces between regions of condensed polarization similar to ferroelectric domains. (iv) Finally, saturation of the second harmonic signal below T_f (state s

in Fig. 1) is consistent with total freezing of the polarization dynamics, perhaps due to the pinning of the interfaces.

In conclusion, the present HRS experiments give a new perspective for understanding the THz-frequency polarization dynamics of perovskite relaxors. The temperature behavior of the ferroelectric soft mode and its components is described in the full temperature range and it is related to the dielectric permittivity via a phenomenological model. Singlet-doublet splitting of the ferroelectric soft mode is observed only up to about 400 K, i.e., only in the relaxor ice and the relaxor liquid states. At higher temperatures, a new picture of the *single paraelectriclike soft mode* interacting with a disorder-induced hard mode is proposed. This picture allows us to explain the temperature dependence of the hyper-Raman spectra of both PMN and PMT, and very likely in the other perovskite relaxors as well. This extraneous spectral feature, here identified as a hard, Raman-active mode, arises probably due to antiferroelectric vibrations similar to the F_{2g} mode of the hypothetical $Fm\bar{3}m$-symmetry chemically ordered cluster, but the precise clarification of its microscopic nature still remains a challenge for future atomistic modeling.

One of us (J. H.) would like to thank the Czech Science Foundation for its support of this work (Project No. 15-04121S).

*bernard.hehlen@umontpellier.fr
†hlinka@fzu.cz

[1] R. A. Cowley, S. N. Gvasaliya, S. G. Lushnikov, B. Roessli, and G. M. Rotaru, Adv. Phys. **60**, 229 (2011).
[2] L. E. Cross, Ferroelectrics **76**, 241 (1987).
[3] R. Blinc, *Advanced Ferroelectricity* (Oxford University Press, New York, 2011).
[4] J. Hlinka, J. Petzelt, S. Kamba, D. Noujni, and T. Ostapchuk, Phase Transitions **79**, 41 (2006).
[5] I. Grinberg, Y.-H. Shin, and A. M. Rappe, Phys. Rev. Lett. **103**, 197601 (2009).
[6] Z.-G. Ye, Key Eng. Mater. **155**, 81 (1998).
[7] A. E. Glazounov and A. K. Tagantsev, Appl. Phys. Lett. **73**, 856 (1998).
[8] R. Pirc and R. Blinc, Phys. Rev. B **76**, 020101(R) (2007).
[9] J. Hlinka, J. Adv. Dielectr. **02**, 1241006 (2012).
[10] A. Bosak, D. Chernyshov, S. Vakhrushev, and M. Krisch, Acta Crystallogr. Sect. A **68**, 117 (2012).
[11] A. Al-Barakaty, S. Prosandeev, D. Wang, B. Dkhil, and L. Bellaiche, Phys. Rev. B **91**, 214117 (2015).
[12] H. Takenaka, I. Grinberg, and A. M. Rappe, Phys. Rev. Lett. **110**, 147602 (2013).
[13] V. V. Shvartsman, A. L. Kholkin, A. Orlova, D. Kiselev, A. Bogomolov, and A. Sternberg, Appl. Phys. Lett. **86**, 202907 (2005).
[14] P. Bonneau, P. Garnier, G. Calvarin, E. Husson, J. R. Gavarri, A. W. Hewat, and A. Morell, J. Solid State Chem. **91**, 350 (1991).
[15] R. Pattnaik and J. Toulouse, Phys. Rev. Lett. **79**, 4677 (1997).
[16] M. A. Akbas and P. K. Davies, J. Am. Ceram. Soc. **80**, 2933 (1997).
[17] A. Levstik, Z. Kutnjak, C. Filipic, and R. Pirc, Phys. Rev. B **57**, 11204 (1998).
[18] R. Blinc, J. Dolinsek, A. Gregorovic, B. Zalar, C. Filipic, Z. Kutnjak, A. Levstik, and R. Pirc, Phys. Rev. Lett. **83**, 424 (1999).
[19] R. Fisch, Phys. Rev. B **67**, 094110 (2003).
[20] D. Sherrington, Phys. Rev. B **89**, 064105 (2014).
[21] G. G. Guzman-Verri, P. B. Littlewood, and C. M. Varma, Phys. Rev. B **88**, 134106 (2013).
[22] M. Pasciak, T. R. Welberry, J. Kulda, M. Kempa, and J. Hlinka, Phys. Rev. B **85**, 224109 (2012).
[23] A. Naberezhnov, S. B. Vakhrushev, B. Dorner, D. Strauch, and H. Moudden, Eur. Phys. J. B **11**, 13 (1999).
[24] M. Tachibana and E. Takayama-Muromachi, Phys. Rev. B **79**, 100104(R) (2009).
[25] C. Stock, L. Van Eijck, P. Fouquet, M. Maccarini, P. M. Gehring, G. Xu, H. Luo, X. Zhao, J.-F. Li, and D. Viehland, Phys. Rev. B **81**, 144127 (2010).
[26] P. Ondrejkovic, M. Kempa, J. Kulda, B. Frick, M. Appel, J. Combet, J. Dec, T. Lukasiewicz, and J. Hlinka, Phys. Rev. Lett. **113**, 167601 (2014).
[27] G. Burns and F. H. Dacol, Solid State Commun. **48**, 853 (1983).
[28] D. Viehland, S. J. Jang, L. E. Cross, and M. Wuttig, Phys. Rev. B **46**, 8003 (1992).
[29] B. Dkhil, P. Gemeiner, A. Al-Barakaty, L. Bellaiche, E. Dul'kin, E. Mojaev, and M. Roth, Phys. Rev. B **80**, 064103 (2009).
[30] P. M. Gehring, H. Hiraka, C. Stock, S.-H. Lee, W. Chen, Z.-G. Ye, S. B. Vakhrushev, and Z. Chowdhuri, Phys. Rev. B **79**, 224109 (2009).
[31] O. Svitelskiy, J. Toulouse, G. Yong, and Z.-G. Ye, Phys. Rev. B **68**, 104107 (2003).
[32] S. Prosandeev, I. P. Raevski, M. A. Malitskaya, S. I. Raevskaya, H. Chen, C.-C. Chou, and B. Dkhil, J. Appl. Phys. **114**, 124103 (2013).
[33] E. Smirnova, A. Sotnikov, S. Ktitorov, N. Zaitseva, H. Schmidt, and M. Weihnacht, J. Appl. Phys. **115**, 054101 (2014).
[34] V. Westphal, W. Kleemann, and M. D. Glinchuk, Phys. Rev. Lett. **68**, 847 (1992).
[35] P. M. Gehring, S. Wakimoto, Z.-G. Ye, and G. Shirane, Phys. Rev. Lett. **87**, 277601 (2001).
[36] I. P. Swainson, C. Stock, P. M. Gehring, G. Xu, K. Hirota, Y. Qiu, H. Luo, X. Zhao, J.-F. Li, and D. Viehland, Phys. Rev. B **79**, 224301 (2009).
[37] J. Hlinka, S. Kamba, J. Petzelt, J. Kulda, C. A. Randall, and S. J. Zhang, Phys. Rev. Lett. **91**, 107602 (2003).
[38] S. B. Vakhrushev and S. M. Shapiro, Phys. Rev. B **66**, 214101 (2002).
[39] S. B. Vakhrushev, R. G. Burkovsky, S. Shapiro, and A. Ivanov, Phys. Solid State **52**, 889 (2010).
[40] H. Taniguchi, M. Itoh, and D. Fu, J. Raman Spectrosc. **42**, 706 (2011).
[41] V. Bovtun, S. Veljko, S. Kamba, J. Petzelt, S. B. Vakhrushev, Y. Yakymenko, K. Brinkman, and N. Setter, J. Eur. Ceram. Soc. **26**, 2867 (2006).
[42] V. N. Denisov, B. N. Marvin, and V. B. Podobedov, Phys. Rep. **151**, 1 (1987).
[43] H. Vogt, Phys. Rev. B **38**, 5699 (1988).
[44] J. Hlinka, B. Hehlen, A. Kania, and I. Gregora, Phys. Rev. B **87**, 064101 (2013).

[45] A. Al-Zein, J. Hlinka, J. Rouquette, and B. Hehlen, Phys. Rev. Lett. **105**, 017601 (2010).
[46] B. Hehlen, G. Simon, and J. Hlinka, Phys. Rev. B **75**, 052104 (2007).
[47] A. Al-Zein, B. Hehlen, J. Rouquette, and J. Hlinka, Phys. Rev. B **78**, 134113 (2008).
[48] J. Hlinka, T. Ostapchuk, D. Noujni, S. Kamba, and J. Petzelt, Phys. Rev. Lett. **96**, 027601 (2006).
[49] S. Wakimoto, C. Stock, R. J. Birgeneau, Z.-G. Ye, W. Chen, W. J. L. Buyers, P. M. Gehring, and G. Shirane, Phys. Rev. B **65**, 172105 (2002).
[50] S. N. Gvasaliya, B. Roessli, R. A. Cowley, P. Huber, and S. G. Lushnikov, J. Phys. Condens. Matter **17**, 4343 (2005).
[51] J. Hlinka, J. Petzelt, B. Brezina, and R. Currat, Phys. Rev. B **66**, 132302 (2002).
[52] J. Weerasinghe, L. Bellaiche, T. Ostapchuk, P. Kuzel, C. Kadlec, S. Lisenkov, I. Ponomareva, and J. Hlinka, MRS Commun. **3**, 41 (2013).
[53] S. A. Prosandeev, E. Cockayne, B. P. Burton, S. Kamba, J. Petzelt, Yu. Yuzyuk, R. S. Katiyar, and S. B. Vakhrushev, Phys. Rev. B **70**, 134110 (2004).
[54] H. Ohwa, M. Iwata, H. Orihara, N. Yasuda, and Y. Ishibashi, J. Phys. Soc. Jpn. **70**, 3149 (2001).
[55] S. G. Lushnikov, S. N. Gvasaliya, and I. G. Siny, Physica (Amsterdam) **263B–264B**, 286 (1999).
[56] M. Kopecký, J. Kub, J. Fábry, and J. Hlinka, Phys. Rev. B **93**, 054202 (2016).
[57] J. Hlinka, T. Ostapchuk, D. Nuzhnyy, J. Petzelt, P. Kuzel, C. Kadlec, P. Vanek, I. Ponomareva, and L. Bellaiche, Phys. Rev. Lett. **101**, 167402 (2008).
[58] J. Toulouse, Ferroelectrics **369**, 203 (2008).